Chemical Science

EDGE ARTICLE

View Article Online
View Journal | View Issue

Cite this: *Chem. Sci.*, 2014, **5**, 951

NiTi-Layered double hydroxides nanosheets as efficient photocatalysts for oxygen evolution from water using visible light†

Yufei Zhao,[abc] Bei Li,[a] Qiang Wang,[d] Wa Gao,[a] Chengle J. Wang,[b] Min Wei,*[a] David G. Evans,[a] Xue Duan[a] and Dermot O'Hare*[b]

Received 10th September 2013
Accepted 22nd October 2013

DOI: 10.1039/c3sc52546e

www.rsc.org/chemicalscience

NiTi-Layered double hydroxides (LDH) nanosheets with lateral dimensions in the range 30–60 nm have been prepared using a reverse microemulsion method. These materials exhibit excellent photocatalytic activity (~2148 μmol g^{-1} h^{-1}) for oxygen evolution from water using visible light. The quantum yield was found to be 65.0% and 20.0% using monochromatic irradiation at 400 and 650 nm respectively.

Introduction

The search for suitable semiconductors that can act as photocatalysts for the splitting of water using solar energy is one of the most important areas of contemporary physical science.[1,2] The formation of oxygen from water is challenging since it has to occur through several steps requiring four positive holes and the formation of O–O bonds.[3] TiO_2-based photocatalysts have been extensively studied for their activity for splitting water into oxygen, but the large band gap of TiO_2 (>3 eV) ensures that it is only photoactive under UV-irradiation.[4] The introduction of dopants has been demonstrated to be an effective approach to extend the activity of TiO_2 into the visible-light region. However, a decrease in photocatalytic efficiency occurs since these dopants generally act as charge carrier recombination centres.[5] Recently, novel approaches based on creating Ti^{3+} centres have been proposed in order to overcome this limitation by narrowing the band gap of semiconductor.[6–8] Frei *et al.* demonstrated a new class of heterobimetallic photocatalysts containing Ti^{3+} active sites for O_2 generation under visible-light.[7,9] However, the photocatalytic efficiency of these materials is still needs to be improved, owing to the low concentration of Ti^{3+} active sites.[10a] Therefore, to meet the requirements for efficient water splitting, the development of new materials or methodologies for obtaining high-performance visible-light photocatalysts remains a tremendous goal.

Layered double hydroxides (LDHs) are a class of 2D inorganic layered matrices,[11–15] which have been widely used in photocatalysis,[14–17] dye-sensitised solar cells,[18] adsorption,[19] CO_2 adsorbents,[20,21] and functional materials.[22,23] Garcia *et al.* firstly reported the high photocatalytic activity of the ZnCr-LDHs, which evokes research interest in LDH materials as photocatalysts.[17] In our previous work, we have demonstrated that Ti-containing LDHs display good photocatalytic activity for water splitting into hydrogen upon UV-visible irradiation.[24] This is attributed to the abundant Ti–O surface defects serving as trapping sites to improve the electron–hole separation. However, we are still to develop controls on both the defect type and concentration in order to make further advances, as well as to extend the photoresponse to visible-light region. It is reported that the size, shape and morphology of semiconductors are key factors in determining their surface defects, which affects both the efficiency of charge separation and the photoconversion capability.[10b–e] Therefore, we have sought to tune the defect type and concentration in Ti-based LDH materials *via* a bottom-up synthesis approach, which would enhance both the efficiency of electron–hole separation and the resulting visible-light photocatalytic oxygen performance.

Herein, we report a facile and efficient synthesis of visible-light responsive NiTi-LDHs nanosheets.[25–27] These nanosheets demonstrate extraordinarily high photocatalytic activity for oxygen evolution from water (~2148 μmol g^{-1} h^{-1}), which we believe is currently the most effective visible-light photocatalyst reported for O_2 production. The reverse microemulsion method is an effective method for controlling the size, shape and morphology of the LDH particles at the nanoscale. The density of Ti^{3+} defects increases gradually upon decreasing the NiTi-

[a]*State Key Laboratory of Chemical Resource Engineering, Beijing University of Chemical Technology, Beijing 100029, P. R. China. E-mail: weimin@mail.buct.edu.cn; Fax: +86-10-64425385; Tel: +86-10-64412131*

[b]*Chemistry Research Laboratory, Department of Chemistry, University of Oxford, Mansfield Road, Oxford OX1 3TA, UK. E-mail: dermot.ohare@chem.ox.ac.uk; Tel: +44 (0)1865 272686*

[c]*Key Laboratory of Photochemical Conversion and Optoelectronic Materials, Technical Institute of Physics and Chemistry, Chinese Academy of Sciences, Beijing, 100190, P. R. China*

[d]*College of Environmental Science and Engineering, Beijing Forestry University, Qinghua East Road, Haidian District, Beijing 100083, P. R. China*

† Electronic supplementary information (ESI) available: Sample characterization, photocatalytic reaction of splitting water into oxygen, the detailed calculation information about the apparent QY, computational details for band structure, and additional characterization data. See DOI: 10.1039/c3sc52546e

LDH nanosheets from 90 to 30 nm. The photoluminescence measurements indicate an effective electron–hole separation, which is attributed to the abundant surface Ti^{3+} defects serving as trapping sites which we have confirmed by ESR and EXAFS measurement. UV-vis absorption measurements reveal that the absorption edge for the NiTi-LDH nanosheets shifts to longer wavelengths compared with a conventional microcrystalline LDH sample, this observation was supported by periodic density functional (DFT) theoretical calculations which predicts a decrease of ~1.8 eV in the band gap. This work demonstrates that controlling the particle size and surface defects in NiTi-LDHs is a promising strategy for the improvement of the visible-light photocatalytic behavior for both water splitting and solar energy conversion.

Experimental section

Materials

Chemical reagents including $Ni(NO_3)_2 \cdot 6H_2O$, $NiCl_2 \cdot 6H_2O$, titanium propoxide, $TiCl_4$, urea, sodium dodecyl sulfate, isooctane, TiO_2 (rutile), WO_3 were purchased from Sigma-Aldrich Co. $Cr(NO_3)_3 \cdot 9H_2O$, $Zn(NO_3)_2 \cdot 6H_2O$, NaOH, Na_2CO_3 were obtained from Beijing Chemical Co., Ltd. Deionised and decarbonated water was used in all the experimental processes.

Synthesis of NiTi-LDH nanosheets using the reverse micelle method

NiTi-LDH nanosheets with different particle size were prepared by using the reverse microemulsion method reported by the O'Hare group.[25] Typically, sodium dodecyl sulfate (1.08 g for NiTi-LDH-1, 0.72 g for NiTi-LDH-2), isooctane (50 mL) and deionised water (1.1 mL) were mixed in a flask with magnetic stirring, and 1-butanol (1.5 mL) was added dropwise until the reverse microemulsion was stable and transparent. $Ni(NO_3)_2 \cdot 6H_2O$ (1.164 g, 0.004 mol) and $TiCl_4$ (0.11 mL, 0.001 mol) were then added into the microemulsion and stirred for one hour. Finally, urea (1.2 g) was added into the mixture and the resulting solution was aged at 110 °C for 27 h with refluxing and stirring. The precipitate was collected by centrifuging, washed thoroughly with a mixture solvent of ethanol and water (1 : 1, v/v) for several times and finally air-dried. NiTi-LDH nanosheets containing different molar ratios of Ni^{2+}/Ti^{4+} were prepared by using the same method using different stoichiometric ratios.

Synthesis of NiTi-LDH powdered material using the coprecipitation method

The NiTi-LDH-3 sample was prepared by coprecipitation. In brief, a 0.5 mL $TiCl_4$: HCl solution {1 : 1 (v/v)}, $Ni(NO_3)_2 \cdot 6H_2O$ (0.008 mol), and urea (0.1 mol) were dissolved in deionised water (100 mL) under vigorous stirring for 27 h at refluxing temperature (100 °C). The resulting solid was centrifuged, washed thoroughly and dried at 60 °C.

The synthesis of NiTi-LDH-4 sample was similar to that described by Kang *et al.*[28] Titanium propoxide (0.0013 mol), $NiCl_2 \cdot 6H_2O$ (0.008 mol), and urea (0.1 mol) were dissolved in deionized water (100 mL) under vigorous stirring for 46 h at refluxing temperature (90 °C). The resulting solid was centrifuged, washed and finally dried at 60 °C.

For comparison, a sample of ZnCr-LDH, was prepared using the coprecipitation method reported by Garcia *et al.*[17]

Results and discussion

Structure and morphology of the NiTi-LDH materials

The XRD patterns of the synthesised NiTi-LDH-*n* (n = 1–4) are shown in Fig. S1A.† In each case, the Bragg reflections can be indexed to a unit cell with rhombohedral *R*3*m* symmetry, commonly used for the description of LDH structures.[29] The basal spacing of these LDHs is 0.716 nm, close to the value of found for CO_3^{2-}-containing LDHs. For the NiTi-LDH-*n* (n = 1, 2) (*i.e.* samples prepared by reverse micelle method), the Bragg reflections are significantly broader and weaker than for the bulk NiTi-LDH-*n* (n = 3, 4) samples synthesised by conventional coprecipitation method, indicating the smaller particle size and poorer crystallinity for the former two samples. The nature of interlayer anions in NiTi-LDH-*n* was investigated using FT-IR spectroscopy (Fig. S1B†). An intense IR absorption band at 2235 cm^{-1} can be assigned to the antisymmetric stretching vibration (ν_{CN}) of the cyanate anion (CNO^-), which results from the incomplete decomposition of urea;[28] an absorption band at 1384 cm^{-1} can be assigned to the ν_3 (asymmetric stretching) mode of the interlayer CO_3^{2-} anions.[24] The data suggests the co-existence of both CNO^- and CO_3^{2-} anions in the NiTi-LDH-*n* (n = 1–4). For NiTi-LDH-*n* (n = 1, 2) the IR spectra provide the evidence of the presence of CH_2, CH_3 (ν_{CH}) in the dodecyl chain (2958, 2918, 2850 cm^{-1}), implying the adsorption of some dodecyl sulfate anions (DDS) onto the surface of NiTi-LDH-*n* (n = 1, 2) sheets. Typical TEM images (Fig. 1A–D) reveal that NiTi-LDH-*n* (n = 1–3) display a plate-like morphology with a lateral dimension of 30 ± 20 nm, 60 ± 20 nm, 90 ± 30 nm, respectively, accompanied with some inevitable aggregation;

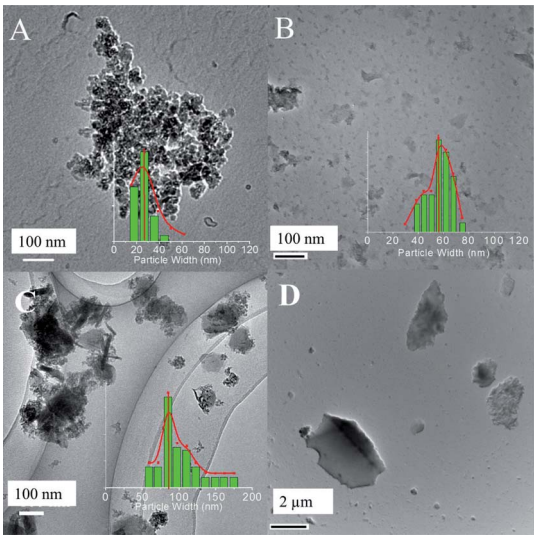

Fig. 1 TEM images of (A) NiTi-LDH-1, (B) NiTi-LDH-2, (C) NiTi-LDH-3, (D) NiTi-LDH-4.

while the NiTi-LDH-4 sample displays rather larger particle size (~2 μm). The restacking of the LDH nanosheets was investigated by atomic force microscopy (AFM) in tapping-mode. As shown in Fig. 2 and Fig. S2,† the nano-sized NiTi-LDH-1 and NiTi-LDH-2 with lateral width of 50–80 nm and thickness of ~2.0 nm are observed from the cross-sectional analysis, and NiTi-LDH-3 and NiTi-LDH-4 show larger particles (~110 nm and ~2.2 μm in lateral size) with thickness of ~15 nm and ~700 nm, respectively. The LDHs diameter is close to the TEM results. Based on the interlayer distance of 0.716 nm from the XRD patterns (Fig. S1†), it is therefore estimated that the NiTi-LDH-*n* ($n = 1$–3) samples consist of ~2, ~3 and ~20 LDH layers; while NiTi-LDH-4 exhibits the largest packing with ~950 layers. We believe the small lateral size and thin nanosheet morphology of NiTi-LDH-*n* ($n = 1$, 2) samples provide a large surface area and sufficient exposure of active centre, facilitating the improvement of photocatalytic behavior.

The surface area and pore-size distribution of the nanosheets and bulk samples were investigated by N_2-adsorption/desorption measurement (Fig. S3†). In the cases of NiTi-LDH-1 and NiTi-LDH-2, the samples show an isotherm typical of type II with H1-type hysteresis loop, indicative of interparticle mesoporosity. However, NiTi-LDH-3 and NiTi-LDH-4 exhibit typical IV isotherms with H3-type hysteresis loop, implying the presence of mesopores; furthermore, no limiting adsorption at higher P/P_0 was observed, indicating the existence of macropores. This result is further confirmed by the corresponding pore size distribution. In comparison with the NiTi-LDH-3 and NiTi-LDH-4 which show a broader pore distribution, the nano-sized NiTi-LDH-1 and NiTi-LDH-2 give a mesopore distribution in the range 3–6 nm with the maximum at 4 nm. Moreover, a difference in the specific surface area for these LDH materials was also found: the NiTi-LDH-1 shows a larger value (169.0 $m^2\ g^{-1}$); while the NiTi-LDH-*n* ($n = 2$–4) samples exhibit lower values (127.4 $m^2\ g^{-1}$, 91.4 $m^2\ g^{-1}$ and 109.4 $m^2\ g^{-1}$, respectively). The increasing in the specific surface area of NiTi-LDH nanosheets should be preferable for the most efficient exposure of the active sites and the resulting photocatalytic activity.

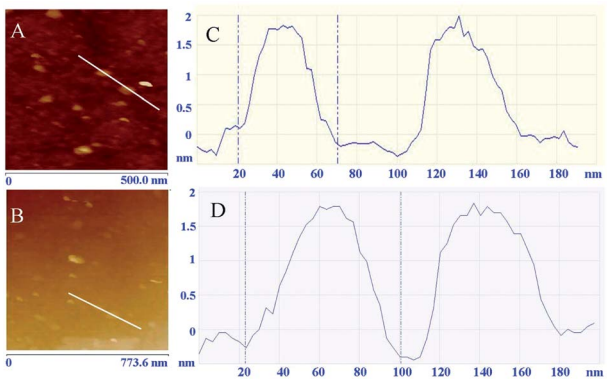

Fig. 2 AFM images of (A) NiTi-LDH-1, (B) NiTi-LDH-2; cross-sectional images of (C) NiTi-LDH-1, (D) NiTi-LDH-2.

Electronic structure of NiTi-LDH materials

The photoluminescence (PL) behavior is related to the transfer of the photoinduced electrons and holes, which can reflect the separation-recombination process of photoinduced charge carriers. In this study, the PL emission spectra of the NiTi-LDH-*n* ($n = 1$–4) samples were examined in the wavelength range 440–510 nm (Fig. 3A). The bulk LDH material (NiTi-LDH-4) shows the strongest PL emission peak at 466 nm ($\lambda_{ex} = 366$ nm); while the emission from the NiTi-LDH-*n* ($n = 1$–3) samples becomes significantly weaker than the bulk one, indicating a depressed rate of electron–hole recombination in the NiTi-LDH nanosheets. This should be beneficial for the photocatalytic performance. In addition, the diffuse reflectance UV-vis spectra of the NiTi-LDH-1 and NiTi-LDH-4 are shown in Fig. 3B. Two absorption bands in the visible region at approximately 400 and 682 nm were observed, which can be attributed to the ligand-to-metal charge transfer and the existence of Ni cation, respectively. A significant red-shift of the absorption edge for the NiTi-LDH-1 and NiTi-LDH-4 sample was found, with respect to TiO_2 as a reference sample. Moreover, the band gap was calculated from the UV–vis diffuse reflectance spectra (Fig. 3B, inset), which shows that the nano-sized NiTi-LDH-1 has a reduced band gap (~2.10 eV) than that of NiTi-LDH-4 (~2.40 eV) and TiO_2 (~3.22 eV). In addition, cyclic voltammetry measurements of these NiTi-LDH materials were performed to analyse their electronic structure, and it was found that both

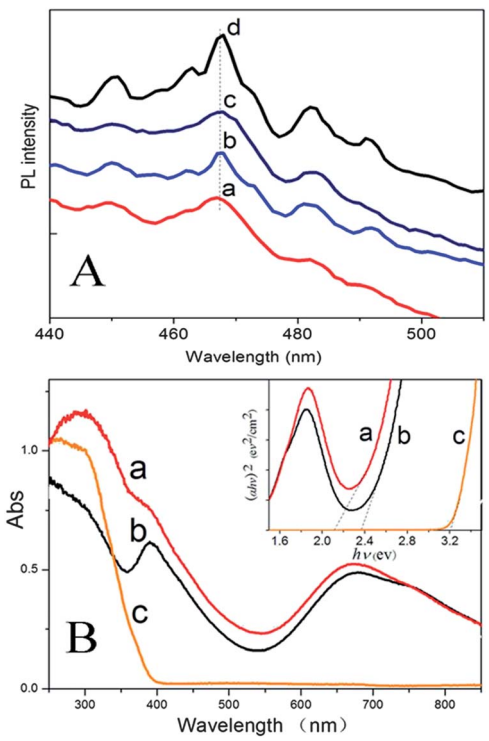

Fig. 3 (A) The fluorescence spectra of (a) NiTi-LDH-1, (b) NiTi-LDH-2, (c) NiTi-LDH-3, (d) NiTi-LDH-4 ($\lambda_{ex} = 366$ nm). (B) UV–vis diffuse reflectance spectra of (a) NiTi-LDH-1, (b) NiTi-LDH-4, (c) TiO_2. The inset in B shows their corresponding plots of $(\alpha h\nu)^2$ *vs.* $h\nu$ for the determination of the direct band gap.

the oxidation and reduction electric potentials ($E_{onset,ox}$ and $E_{onset,red}$) decrease with the decrease of the particle size (Fig. S4†). Accordingly, on the basis of the empirical relationships proposed by deLeeuw *et al.*,[30,31] the frontier orbitals (the highest occupied molecular orbital (HOMO) and lowest unoccupied molecular orbital (LUMO)) energy can be determined as follows:

$$E(\text{HOMO}) = -(E_{onset,ox} + 4.39)\ \text{eV} \quad (1)$$

$$E(\text{LUMO}) = -(E_{onset,red} + 4.39)\ \text{eV} \quad (2)$$

Therefore, the band gap energy can be calculated by $\Delta E_g = E(\text{LUMO}) - E(\text{HOMO})$, which was determined to be ~1.98 eV (NiTi-LDH-1), ~2.05 eV (NiTi-LDH-2), ~2.11 eV (NiTi-LDH-3) and ~2.23 eV (NiTi-LDH-4), respectively, in agreement with the results of PL and UV-vis spectra. These results demonstrate that the band gap decreases significantly in the nano-sized NiTi-LDH materials compared to the bulk material.

Photocatalytic activity and quantum yields in visible-light water splitting

The photocatalytic activity of the NiTi-LDHs was investigated by monitoring the time-dependent O_2 generation under visible illumination ($\lambda > 400$ nm) using $AgNO_3$ as a sacrificial reagent. As shown in Fig. 4A, the NiTi-LDH materials display photocatalytic activity with the following sequence: NiTi-LDH-1 (~2148 μmol g^{-1} h^{-1}) > NiTi-LDH-2 (~1714 μmol g^{-1} h^{-1}) > ZnCr-LDH (~1098 μmol g^{-1} h^{-1}) > WO_3 (~563 μmol g^{-1} h^{-1}) > NiTi-LDH-3 (~536 μmol g^{-1} h^{-1}) > NiTi-LDH-4 (~267 μmol g^{-1} h^{-1}). Moreover, the NiTi-LDH materials show photoactivity per square meter as follows: NiTi-LDH-2 (~13.45 μmol m^{-2} h^{-1}) > NiTi-LDH-1 (~12.71 μmol m^{-2} h^{-1}) > NiTi-LDH-3 (~5.86 μmol m^{-2} h^{-1}) > NiTi-LDH-4 (~2.44 μmol m^{-2} h^{-1}). The results show that the nano-sized NiTi-LDHs exhibit largely-enhanced photocatalytic activity than that of bulk LDH as well as ZnCr-LDH and WO_3. The water splitting activity of the NiTi-LDHs as a function of Ni/Ti molar ratio was also investigated. The XRD patterns of NiTi-LDH nanosheet containing various Ni/Ti ratios are shown in Fig. S5.† The Bragg reflections may be indexed to an LDH phase for these samples. The NiTi-LDH nanosheets with a Ni : Ti ratio of 4 : 1 displays the highest photocatalytic H_2 production activity (~2148 μmol g^{-1} h^{-1}), in comparison with a LDH with a Ni : Ti ratio of 2 : 1 (~1043 μmol g^{-1} h^{-1}), 3 : 1 (~1963 μmol·$g^{-1}h^{-1}$), and 5:1 (~1577 μmol g^{-1} h^{-1}), respectively (Fig. S6†). Table S1† summaries many of the previously reported photocatalysts for water splitting.[17,32] These data suggest that NiTi-LDH-1 is currently the most efficient visible-light photocatalyst for photoinduced O_2 production from water. In addition, the lifetime and reproducibility of the photoactivity of NiTi-LDH-1 has been evaluated, these samples show a constant photocatalytic activity (~2100 μmol g^{-1} h^{-1}) over 3 consecutive cycles (Fig. 4B). The fate of the metallic Ag derived from the $AgNO_3$ sacrificial reagent was studied by HRTEM (Fig. S7†). The HRTEM images show that Ag nanoparticles (NPs) are deposited on the surface of LDH nanosheets. The NPs gradually increase in density from the 1st to 3rd cycle without an obvious change in the NP particle size (4–12 nm). The deposited Ag NPs may not impose great influence on the reproducible light absorption and photocatalytic activity.

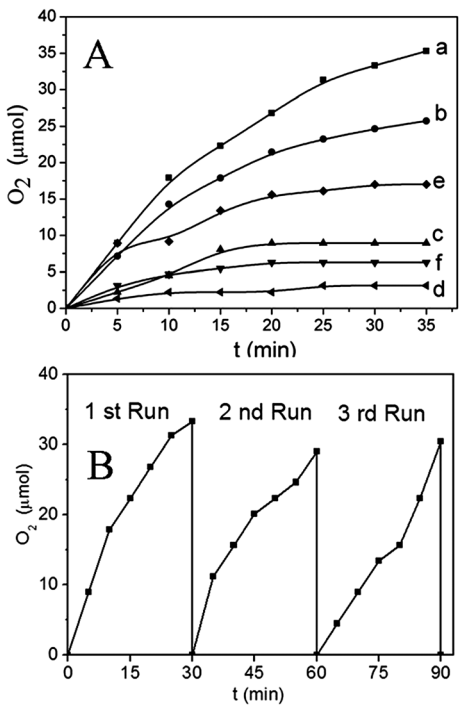

Fig. 4 (A) O_2 evolution from aqueous solution using 10^{-2} M $AgNO_3$ as the sacrificial acceptor under visible-light: (a) NiTi-LDH-1, (b) NiTi-LDH-2, (c) NiTi-LDH-3, (d) NiTi-LDH-4, (e) ZnCr-LDH, (f) WO_3. (B) Catalyst cycling for the photocatalytic generation of oxygen in water in the presence of NiTi-LDH-1.

To optimize the oxygen generation by NiTi-LDH-1, we determined the O_2 volume as a function of time with various photocatalyst concentration (0.5 to 2 g L^{-1}). As shown in Fig. S8,† a concentration of 1 g L^{-1} was found to give the highest photocatalytic activity (~2148 μmol g^{-1} h^{-1}). The quantum yield (QY) for incident photon to oxygen conversion is an important parameter to establish the photocatalytic efficiency especially in the visible-light region. The apparent QY for O_2 generation was tested by using monochromatic light of wavelengths corresponding to the maxima of the absorption bands based on concentration of 1 g L^{-1} (details of the calculation of the apparent QY are described in SI). As shown in Fig. 5, using potassium ferrioxalate as a chemical actinometer, a QY of ~65.0% and ~20.0% was obtained for the NiTi-LDH-1 sample under monochromatic irradiation at 400 and 650 nm, respectively. The different QY at various visible absorption bands is due to the different nature of the electronic transition promoted at each wavelength. To the best of our knowledge, this is the highest QY reported for photocatalytic generation of O_2 under visible-light irradiation (as shown in Table S1†).[32] The results indicate that the nano-sized NiTi-LDH materials prepared by the reverse microemulsion method are very promising visible-light photocatalyst for oxygen evolution from water, with high activity, efficiency, long-term stability and recyclability.

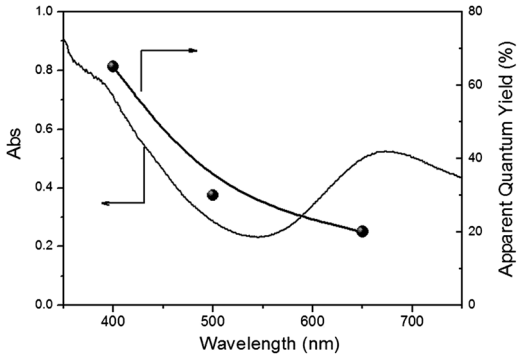

Fig. 5 Diffuse reflectance UV-vis spectra (plotted as the Kubelka-Munk function of the reflectance) of NiTi-LDH-1 and observed quantum yield for oxygen evolution.

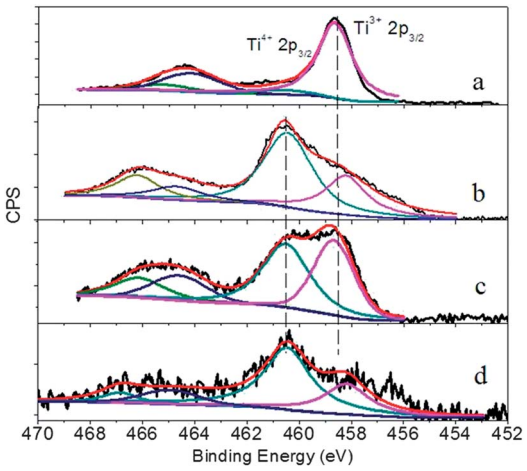

Fig. 6 Ti 2p XPS-spectra of (a) NiTi-LDH-1, (b) NiTi-LDH-2, (c) NiTi-LDH-3, (d) NiTi-LDH-4.

Structure–property correlations

In order to explore the redox ability of the Ti-containing LDH nanosheets, ESR spectroscopy was carried out to help give an insight into the chemical surroundings of Ti in NiTi-LDHs (Fig. S9†). The fresh sample of NiTi-LDH-1 exhibits two major signal at g values of 1.996 (curve a, Section A) and 2.030 (curve a, Section B) respectively. These signals can be assigned to Ti^{3+} species and O^- according to their reported values.[33] Upon visible-light exposure for 0.5 h, the signal due to Ti^{3+} increases together with the appearance of a new signal at 2.008 which may attributed to O_2^-,[34,35] No Ti^{3+} signal was detected by ESR from the bulk sample NiTi-LDH-4 (Fig. S10†), a weak Ti^{3+} signal for NiTi-LDH-4 could be due to its lower surface area and thereby reduced concentration of surface Ti^{3+} sites. Kong *et al.* reported that the increased ratio of surface defects for TiO_2 nanocrystals can significantly improve the separation efficiency of the photo-generated electron–hole and the resulting photocatalytic activity.[36a] For the NiTi-LDH nanosheets, it is therefore proposed that the Ti^{3+} species play the key role of trapping sites for electrons, which facilitates the visible-light catalytic performance.

X-ray photoelectron spectroscopy (XPS) is a well-established surface analysis technique, which was used to determine Ti oxidation states in NiTi-LDHs. As shown in Fig. 6d, the XPS spectrum of NiTi-LDH-4 (Ti $2p_{3/2}$) exhibits two peaks at 458.6 eV and 460.5 eV, corresponding to the binding energy of Ti^{3+} and Ti^{4+}, respectively. It should be noted that this sample displays a large particle size (lateral size: ~2.2 μm; thickness: ~700 nm), which would lead to a low density of surface Ti species and the resulting low signal-to-noise in XPS spectrum. In the cases of NiTi-LDH-n (n = 1–3) nanosheets (Fig. 6a–c), with the decrease of particle size, the Ti^{3+} defect ($2p_{3/2}$ peak at 458.6 eV) increases significantly accompanied with a concomitant decrease in the Ti^{4+} signal (460.5 eV). A quantitative analysis of Ti^{4+} and Ti^{3+} surface states for the LDH samples are presented as Table 1. It was found that the density of the Ti^{3+} sites increases markedly upon decreasing the NiTi-LDH particle size from 2 μm to 30 nm. The Ti^{3+} surface states for NiTi-LDH-1 account for ~88.0% (molar percentage), in contrast to ~27.3% of the NiTi-LDH-4 sample. The increased concentration of surface Ti^{3+} sites in NiTi-LDH-1 can be attributed to the particle size effect. The chemical composition of the LDH samples is listed in Table S2.† It has been reported that a larger fraction of Ti^{3+} results in more oxygen defects,[6,36b–d] which imposes a significant impact on the electronic properties and favors the efficient separation of electron–hole pair.[36e] Therefore, the red-shift in the band gap of nano-sized NiTi-LDH-1 observed in this work can be attributed to the formation of these Ti^{3+} and oxygen defects. Visible-light absorption results in promotion of electrons from the band gap localized states, these subsequently react with the electron-acceptor $AgNO_3$, leaving holes trapped on surface hydroxyl sites,[37] which promotes the oxidation of water.[38]

Table 1 The quantitative analysis of Ti^{3+} surface state in Ti 2p of NiTi-LDHs based on the results of XPS

Sample	Particle size	Ti^{3+} concentration (molar percentage)
NiTi-LDH-1	~30 nm	88.0%
NiTi-LDH-2	~60 nm	42.7%
NiTi-LDH-3	~90 nm	47.0%
NiTi-LDH-4	~2 μm	27.3%

The X-ray absorption near-edge structures (XANES) at the Ti K-edge of the samples (NiTi-LDH-1, NiTi-LDH-4 and rutile TiO_2) are shown in Fig. 7. The pre-edge features can provide sensitive information about the symmetry of the titanium environment in these materials. In the case of an octahedral environment, the pre-edge features give rise to three features usually denoted as P_1, P_2 and P_3 corresponding to the quadruple-allowed 1s → 3d transitions (Fig. 7A). The NiTi-LDH-1 exhibits a maximum peak at ~4987.4 eV, 1.1 eV lower than the reference sample (NiTi-LDH-4: 4988.5 eV). The decreased absorption energy indicates a decrease in the oxidation state of Ti^{4+}, which have been previously observed in Ti K-edge XANES spectra.[39,40] The results suggest that the Ti species in NiTi-LDH-1 probably exists as a lower oxidation state (Ti^{d+}, $3 < d < 4$), which is consistent with the XPS results. In addition, the $k2$-weighted Fourier transform of the Ti K-edge EXAFS spectrum of these materials is shown in Fig. 7B, the corresponding refined local structure

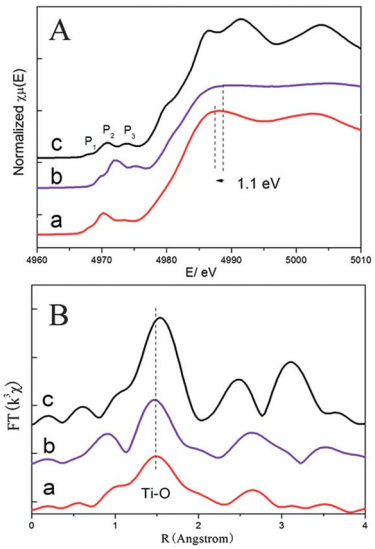

Fig. 7 (A) Ti K-edge, XANES spectra and (B) magnitude of $k2$-weighted Fourier transforms of Ti K-edge EXAFS spectra for of (a) NiTi-LDH-1, (b) NiTi-LDH-4 and (c) rutile TiO_2.

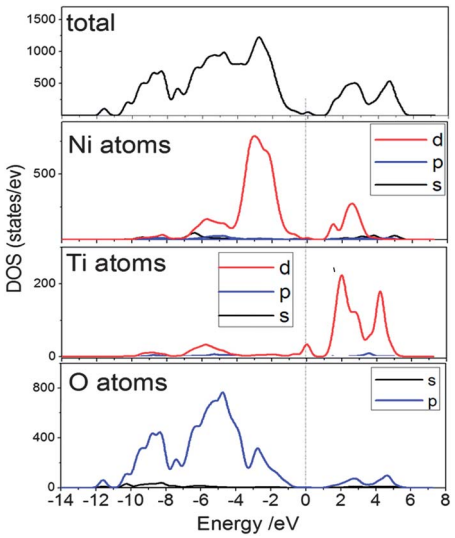

Fig. 8 Total and partial electronic density of states (TDOS and PDOS) for the Ti^{3+}-doped NiTi-LDH system. The Fermi energy level E_F was set to zero.

Table 2 Summary of the local structure around Ti from refinement of the Ti K-edge EXAFS data

Sample	Shell	N^a	R [Å]^b	σ^2 [Å^2]^c	ΔE_0 [eV]^d
TiO_2	Ti–O	6.00^e	1.96		3.07
NiTi-LDH-4	Ti–O	4.70	1.92	0.008	0.20
NiTi-LDH-1	Ti–O	4.33	1.95	0.009	2.89

^{a} N = coordination number. ^{b} R = distance between absorber and backscatter atoms. ^{c} σ^2 = Debye–Waller factor. ^{d} ΔE_0 = energy shift; R space fit, Δk = 2.9–11.4 Å^{-1}, Δr = 0.98–2.07 Å. ^{e} Fixed as 6 for the first TiO_6 shell.

parameters around Ti are listed in Table 2. The first shell of rutile TiO_2 represents the nearest-neighbour Ti–O coordination sphere with an average distance of 1.96 Å and coordination number of 6.00 (curve a). However, distinct variations were observed for the NiTi-LDH materials. The first shell in the $k2$-weighted Fourier transform of the Ti K-edge EXAFS spectrum of NiTi-LDH-4 (Fig. 7B, curve b) is at a distance of 1.92 Å with a coordination number of 4.70, can be assigned to the Ti–O octahedra in the LDH layers, both of which are less than those of TiO_2. In the case of NiTi-LDH-1 sample (Fig. 7B, curve a), further structure distortions in the Ti–O distance (1.95 Å) and coordination number (4.33) are observed. In addition, the Debye–Waller factor (0.009 Å) for the Ti–O bonds for NiTi-LDH-1 is larger than that of NiTi-LDH-4 (0.008), suggesting a more distorted octahedral coordination of Ti in NiTi-LDH-1.[41–43] The EXAFS study implies that upon decreasing particle size of the NiTi-LDH, the concentration of Ti^{3+} site increases along with some structural distortions. Based on the results above, the increased concentration of Ti^{3+} defects is in accordance with the results of PL behavior and UV-vis spectra.

To further study the electronic structure of Ti^{3+} in these NiTi-LDHs, periodic density functional (DFT) calculations were carried out for the NiTi-LDH systems. The NiTi-LDH with Ti^{3+} state was introduced by removing oxygen atoms from the central surface, thereby creating a V_{Ti}^{3+} defect (Scheme S1†). Total electronic densities of states (TDOS) and partial electronic densities of states (PDOS) analysis (Fig. S11†) reveal that for an ideal NiTi-LDH system, the VB top is primarily constructed by the occupied Ni 3d and O 2p orbitals while the CB bottom is mainly dominated by the unoccupied Ti 3d orbitals; the band gap transitions from the VB top (highest occupied molecular orbital; HOMO) to the CB bottom (lowest unoccupied molecular orbital; LUMO) is ~2.1 eV. In the case of NiTi-LDH with Ti^{3+} defects, however, the CB bottom is hybridised from both O 2p orbitals and Ti 3d orbitals (Fig. 8), and the band gap was calculated to be ~1.8 eV, much lower than that of the ideal NiTi-LDH system (~2.1 eV). This indicates that the Ti^{3+}-doped LDH exhibits a much wider optical response to solar radiation, which is in accordance with the experimental results. The extended energy states, in combination with the energy levels produced by dopants, may serve as dominant centres for optical excitation and relaxation. The results reveal that the surface Ti^{3+} defects could serve as trapping sites to improve the electron–hole separation as evidenced by PL, which therefore enhances the visible-light photocatalytic efficiency.

A proposed scheme that couples the structure and O_2 evolution process is shown in Fig. 9. The nanosheet LDHs contain Ti^{3+} defects and oxygen vacancies (O_v) neighboring the Ti^{3+} site as confirmed by ESR (Fig. S9†). The impurity levels induced by Ti^{3+} self-doping exists in the band gap of LDH as the form of [V_{Ti}^{3+}].[44] Upon visible-light illumination, the electron is excited to an impurity level (the oxygen vacancy trap, Fig. 9A), whose life is much longer than that in the conductive band.[45] This facilitates its interaction with the $AgNO_3$ sacrificial agent, and thus improves the electron–hole separation. The hole left in the valence band accumulates on the surface Ti^{3+} defects, accounting for the enhanced efficiency in water splitting into O_2.

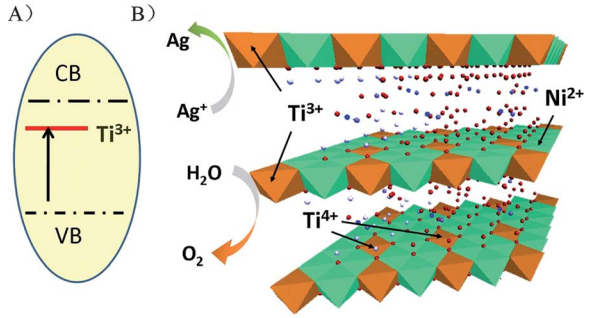

Fig. 9 (A) Proposed structural model of energy states for the Ti^{3+} self-doped NiTi-LDH and (B) schematic illustration of the O_2 evolution process over the NiTi-LDH nanosheet under visible-light irradiation.

Conclusions

In summary, Ti^{3+}-containing NiTi-LDH nanosheets have been synthesised through a reverse microemulsion method. These materials display excellent visible-light photocatalytic activity and recyclability for splitting water into oxygen. The lateral size of LDH nanosheets can be tuned from 60 to 30 nm by increasing the DDS/water ratio, giving a limiting sheet thickness of ~2 nm which corresponds to ~3 stacking repeats. The NiTi-LDH sample (~30 nm) exhibits an extraordinarily high photocatalytic activity for oxygen evolution (~2148 μmol g^{-1} h^{-1}), with a QY of ~65.0% at 400 nm. Currently, one of the most effective visible-light photocatalyst reported for O_2 production. PL spectra demonstrate a weaker electron–hole recombination for the NiTi-LDH nanosheets compared with bulk sample, as a result of abundant Ti^{3+} surface defects serving as trapping sites to facilitate the electron–hole separation. In addition, DFT calculations reveal that the electronic structure of the NiTi-LDH is modified by incorporating Ti^{3+} into the CB structure giving a much reduced band gap. Overall, this work provides a platform for the facile preparation of visible-light responsive photocatalysts for water splitting, which can be used as a promising candidates in the field of solar-energy conversion.

Acknowledgements

This work was supported by the 973 Program (Grant no. 2011CBA00504), the National Natural Science Foundation of China (NSFC), the Scientific Funds from Beijing Municipal Commission of Education (20111001002), the Fundamental Research Funds for the Central Universities and the "Chemical Grid Project" of Beijing University of Chemical Technology. M. Wei appreciates the financial aid from the China National Funds for Distinguished Young Scientists of the NSFC. Q. Wang particularly appreciates the financial aid from the Program for New Century Excellent Talents in University (NCET-12-0787).

Notes and references

1 M. R. Hoffmann, S. T. Martin, W. Choi and D. W. Bahnemann, *Chem. Rev.*, 1995, **95**, 69.
2 (*a*) Y. Hou, F. Zuo, A. Dagg and P. Y. Feng, *Nano Lett.*, 2012, **12**, 6464; (*b*) Y. Chen, J. Zhang, M. Zhang and X. Wang, *Chem. Sci.*, 2013, **4**, 3244.
3 R. Nakamura, A. Okamoto, H. Osawa, H. Irie and K. Hashimoto, *J. Am. Chem. Soc.*, 2007, **129**, 9596.
4 J. Tao, T. Luttrell and M. Batzill, *Nat. Chem.*, 2011, **3**, 296.
5 A. Naldoni, M. Allieta, S. Santangelo, M. Marelli, F. Fabbri, S. Cappelli, C. L. Bianchi, R. Psaro and V. Dal Santo, *J. Am. Chem. Soc.*, 2012, **134**, 7600.
6 F. Zuo, L. Wang, T. Wu, Z. Zhang, D. Borchardt and P. Feng, *J. Am. Chem. Soc.*, 2010, **132**, 11856.
7 R. Nakamura and H. Frei, *J. Am. Chem. Soc.*, 2006, **128**, 10668.
8 W. Lin and H. Frei, *J. Am. Chem. Soc.*, 2005, **127**, 1610.
9 W. Y. Lin and H. Frei, *J. Phys. Chem. B*, 2005, **109**, 4929.
10 (*a*) X. Sun and J. Lin, *J. Phys. Chem. C*, 2009, **113**, 4970; (*b*) J. Pan, G. Liu, G. Q. Lu and H.-M. Cheng, *Angew. Chem., Int. Ed.*, 2011, **50**, 2133; (*c*) N. Wu, J. Wang, D. N. Tafen, H. Wang, J.-G. Zheng, J. P. Lewis, X. Liu, S. S. Leonard and A. Manivannan, *J. Am. Chem. Soc.*, 2010, **132**, 6679; (*d*) Y. Zhao, C. Eley, J. Hu, J. S. Foord, L. Ye, H. He and S. C. E. Tsang, *Angew. Chem., Int. Ed.*, 2012, **51**, 3846; (*e*) A. McLaren, T. Valdes-Solis, G. Li and S. C. Tsang, *J. Am. Chem. Soc.*, 2009, **131**, 12540.
11 M.-Q. Zhao, Q. Zhang, J.-Q. Huang and F. Wei, *Adv. Funct. Mater.*, 2012, **22**, 675.
12 Q. Wang and D. O'Hare, *Chem. Rev.*, 2012, **112**, 4124.
13 F. Geng, R. Ma and T. Sasaki, *Acc. Chem. Res.*, 2010, **43**, 1177.
14 (*a*) J. L. Gunjakar, T. W. Kim, H. N. Kim, I. Y. Kim and S. J. Hwang, *J. Am. Chem. Soc.*, 2011, **133**, 14998; (*b*) J. L. Gunjakar, I. Y. Kim, J. M. Lee, N.-S. Lee and S. J. Hwang, *Energy Environ. Sci.*, 2013, **6**, 1008; (*c*) J. L. Gunjakar, T. W. Kim, I. Y. Kim, J. M. Lee and S. J. Hwang, *Sci. Rep.*, 2013, **3**, DOI: 10.1038/srep02080.
15 M. Shao, J. Han, M. Wei, D. G. Evans and X. Duan, *Chem. Eng. J.*, 2011, **168**, 519.
16 Y. Zhao, M. Wei, J. Lu, Z. L. Wang and X. Duan, *ACS Nano*, 2009, **3**, 4009.
17 C. Gomes Silva, Y. Bouizi, V. Fornes and H. Garcia, *J. Am. Chem. Soc.*, 2009, **131**, 13833.
18 L. Teruel, Y. Bouizi, P. Atienzar, V. Fornes and H. Garcia, *Energy Environ. Sci.*, 2010, **3**, 154.
19 Y. Zhao, S. He, M. Wei, D. G. Evans and X. Duan, *Chem. Commun.*, 2010, **46**, 3031.
20 Q. Wang, H. H. Tay, Z. Zhong, J. Luo and A. Borgna, *Energy Environ. Sci.*, 2012, **5**, 7526.
21 Q. Wang, J. Luo, Z. Zhong and A. Borgna, *Energy Environ. Sci.*, 2011, **4**, 42.
22 D. G. Evans and X. Duan, *Chem. Commun.*, 2006, 485.
23 J. Han, Y. Dou, J. Zhao, M. Wei, D. G. Evans and X. Duan, *Small*, 2013, **9**, 98.
24 Y. F. Zhao, P. Chen, B. Zhang, D. S. Su, S. Zhang, L. Tian, J. Lu, Z. Li, X. Cao, B. Wang, M. Wei, D. G. Evans and X. Duan, *Chem.–Eur. J.*, 2012, **18**, 11949.
25 C. J. Wang, Y. A. Wu, R. M. J. Jacobs, J. H. Warner, G. R. Williams and D. O'Hare, *Chem. Mater.*, 2011, **23**, 171.
26 G. Hu and D. O'Hare, *J. Am. Chem. Soc.*, 2005, **127**, 17808.

27 A. Wongariyakawee, F. Schäeffel, J. H. Warner and D. O'Hare, *J. Mater. Chem.*, 2012, **22**, 7751.
28 Y. Lee, J. H. Choi, H. J. Jeon, K. M. Choi, J. W. Lee and J. K. Kang, *Energy Environ. Sci.*, 2011, **4**, 914.
29 J. Xu, S. Zhao, Z. Han, X. Wang and Y. F. Song, *Chem.–Eur. J.*, 2011, **17**, 10365.
30 D. M. deLeeuw, M. M. J. Simenon, A. R. Brown and R. E. F. Einerhand, *Synth. Met.*, 1997, **87**, 53.
31 D. Yan, J. Lu, J. Ma, M. Wei, X. Wang, D. G. Evans and X. Duan, *Langmuir*, 2010, **26**, 7007.
32 A. Kudo and Y. Miseki, *Chem. Soc. Rev.*, 2009, **38**, 253.
33 (*a*) R. F. Howe and M. Gratzel, *J. Phys. Chem.*, 1987, **91**, 3906–3909; (*b*) H. Liu, H. T. Ma, X. Z. Li, W. Z. Li, M. Wu and X. H. Bao, *Chemosphere*, 2003, **50**, 39.
34 D. Tsukamoto, Y. Shiraishi, Y. Sugano, S. Ichikawa, S. Tanaka and T. Hirai, *J. Am. Chem. Soc.*, 2012, **134**, 6309.
35 L.-B. Xiong, J.-L. Li, B. Yang and Y. Yu, *J. Nanomater.*, 2012, **2012**, 1.
36 (*a*) M. Kong, Y. Li, X. Chen, T. Tian, P. Fang, F. Zheng and X. Zhao, *J. Am. Chem. Soc.*, 2011, **133**, 16414; (*b*) I. Justicia, P. Ordejon, G. Canto, J. L. Mozos, J. Fraxedes, G. A. Battiston, R. Gerbasi and A. Figueras, *Adv. Mater.*, 2002, **14**, 1399; (*c*) S. Hoang, S. P. Berglund, N. T. Hahn, A. J. Bard and C. B. Mullins, *J. Am. Chem. Soc.*, 2012, **134**, 3659; (*d*) V. Ischenko, S. Pozarz, D. Grote, V. Stavarache, K. Fink and M. Driess, *Adv. Funct. Mater.*, 2005, **15**, 1945; (*e*) S. He, S. Zhang, J. Lu, Y. Zhao, J. Ma, M. Wei, D. G. Evans and X. Duan, *Chem. Commun.*, 2011, **47**, 10797.
37 F. E. Osterloh, *Chem. Mater.*, 2008, **20**, 35.
38 D. Brühwiler and H. Frei, *J. Phys. Chem. B*, 2003, **107**, 8547.
39 F. Fang, J. Zhang, J. Zhu, G. R. Chen, D. L. Sun, B. He, Z. Wei and S. Q. Wei, *J. Phys. Chem. C*, 2007, **111**, 3476.
40 Z. W. Huang, X. Gu, Q. Q. Cao, P. P. Hu, J. M. Hao, J. H. Li and X. F. Tang, *Angew. Chem., Int. Ed.*, 2012, **51**, 4198.
41 L. Aimoz, C. Taviot-Guého, S. V. Churakov, M. Chukalina, R. Dähn, E. Curti, P. Bordet and M. Vespa, *J. Phys. Chem. C*, 2012, **116**, 5460.
42 H. Roussel, V. Briois, E. Elkaim, A. de Roy and J. P. Besse, *J. Phys. Chem. B*, 2000, **104**, 5915.
43 Y. Du and D. O'Hare, *Inorg. Chem.*, 2008, **47**, 3234.
44 M. Xing, W. Fang, M. Nasir, Y. Ma, J. Zhang and M. Anpo, *J. Catal.*, 2013, **297**, 236.
45 M. Sugawara, *Phys. Rev. B: Condens. Matter Mater. Phys.*, 1995, **51**, 10743.